Laser and Particle Beams (2016), *34*, 615–620.

doi:10.1017/S0263034616000501

Electrical characterization of atmospheric pressure dielectric barrier discharge-based cold plasma jet using ring electrode configuration

G. DIVYA DEEPAK,[1] N.K. JOSHI,[1] U. PAL,[2] AND R. PRAKASH[2]

[1]Department of Nuclear Science and Technology, Mody University of Science and Technology, Lakshmangarh, Rajasthan 332311, India
[2]Plasma Devices Laboratory, MWT Area, CSIR-Central Electronics Engineering Research Institute, Pilani, Rajasthan 333031, India

(RECEIVED 5 April 2016; ACCEPTED 2 August 2016)

Abstract

In this study, an atmospheric pressure cold plasma jet has been generated based on dielectric barrier discharge plasma. The double ring electrode configuration is used and analysis has been performed subjected to wide range of supply frequencies up to 25 kHz and supply voltage up to 6 kV. The electrical characterization of the plasma jet has been carried out using a high voltage probe. The V-I characteristics of the developed cold plasma jet have been studied and the consumption of the power has been analyzed at various input combinations of supply frequency and applied voltage. Consequently, the supply voltage and supply frequency are optimized with respect to the discharge current and jet length for optimum power consumption. The peak power consumed for glow discharge operation has been found to be 1.27 W in the optimized configuration.

Keywords: Atmospheric pressure plasma jet (APPJ); Dielectric barrier discharge; Jet length; Ring electrode configuration; Supply frequency

1. INTRODUCTION

Atmospheric pressure plasma jets (APPJ) offer a chamberless delivery of downstream reaction, ideal for many applications, such as, material surface treatment, nano-structure fabrication, sterilization, disinfection, and biomedicine (Stevens & Shenton, 2001; Laroussi, 2002; Girard-Lauriaul *et al.*, 2005; Joaquin *et al.*, 2006; Xu *et al.*, 2008). Plasma jets operating with noble gases can be classified into four categories, that is, dielectric-free electrode (DFE) jets, dielectric barrier discharge (DBD) jets, DBD-like jets, and single electrode (SE) jets (Eliasson & Kogelschatz, 1991; Park *et al.*, 1998). Jeong *et al.* (1998) reported the generation of a non-equilibrium APPJ by using a radio frequency discharge device adopting two coaxial metal electrodes, where the plasma jet was sustained by a strong gas flow passing through the discharge region. Liu and Neiger (2003) proposed an electrical model of a DBD for arbitrary excitation voltage. Pal *et al.* (2009) made an effort to understand a single peak discharge phenomenon based on an equivalent circuit model, which has enabled them to characterize DBDs electrically. Furthermore, DBD has been carefully investigated by (Teschke *et al.*, 2005).

Various portable APPJ devices, including jet needle (Bibinov *et al.*, 2007) and plasma pencil (Laroussi & Lu, 2005; Lu & Laroussi, 2006; Xiong *et al.*, 2009) have been constructed. For the effective operation of these APPJ devices often molecular gases, such as oxygen or methane is added to the inert carrying gases (Sanchez-Gonzalez *et al.*, 2007). Kasperczuk *et al.* (2010) investigated interaction of two plasma jets launched successfully at the copper target using PALS iodine laser facility having a beam of diameter 290 mm to understand the process of radiative cooling in plasma jet formation. Li *et al.* (2014) generated a nitrogen based APPJ that was used to treat carbon fiber aluminum composite, which is the most appropriate cathode material to construct the relativistic electron beam sources. Plasma jets generated using different generation techniques are found to exhibit intriguing properties. APPJs overcome the disadvantages of vacuum operation. However, the difficulty of sustaining a glow discharge under these conditions leads to a new set of challenges. Higher voltages are required for gas breakdown

Address correspondence and reprint requests to: G. Divya Deepak, Department of Nuclear Science and Technology, Mody University of Science and Technology, Lakshmangarh, Rajasthan 332311, India. E-mail: divyadeepak77@gmail.com

at 760 torr, and often arcing occurs between the electrodes. So, to prevent arcing, study of physical and chemical properties of APPJs is essential. In this paper, an effort has been made to electrically characterize the DBD-based atmospheric pressure cold plasma jet with respect to supply voltage and frequency to understand the dynamic behavior of APPJs.

2. EXPERIMENTAL SET UP

The double ring electrode configuration is used in this study, which consists of a quartz tube with a nozzle is shown in Figure 1. On top of the nozzle, two metal sleeves are put, which act as the ring electrodes. Out of these, one of the metal sleeves is connected to the supply and other is grounded. Argon gas flows through the inlet of the quartz tube indicated as 1 (see Fig. 1) and its diameter is 22 mm. The diameter of nozzle outlet is 3 mm and has been indicated as 2 (see Fig. 1). The length and outer diameter of the quartz tube are 155 and 25 mm, respectively. The thickness of the quartz tube is 1.5 mm. The axial length and diameter of ring electrodes are 18 and 4 mm respectively. The ring electrodes indicated as 3 are separated by a distance of 3 mm and are clearly shown in Figure 1. A quartz sleeve of 4 mm diameter and 15 mm length was placed on the nozzle of the quartz tube (see Fig. 2) to observe the length of plasma jet without the effect of surrounding air. Jet length has been observed with and without the sleeve.

The double ring electrode configuration is used and subjected to wide range of supply frequencies up to 25 kHz and supply voltages up to 6 kV. Argon was used as the working gas. The plasma jet generated using double ring configuration is shown in Figure 3.

3. RESULTS AND DISCUSSION

The V-I characteristic of the developed DBD-based cold plasma jet has been studied and the consumption of power has been analyzed at various input combinations (supply voltage and frequency). The supply frequency and voltage have been varied from 10 to 25 kHz and 3.5 to 6 kV, respectively. The gas flow rate is fixed at 1 liter/min.

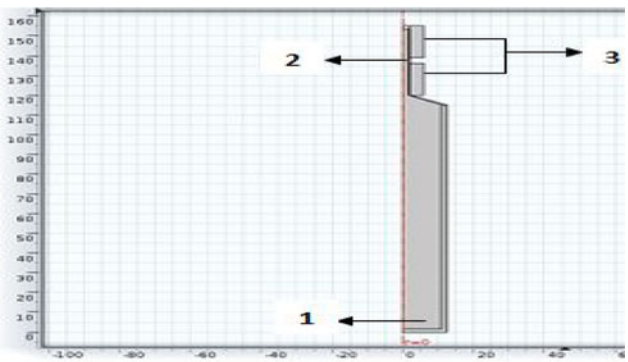

Fig. 1. Geometry of double ring electrode configuration.

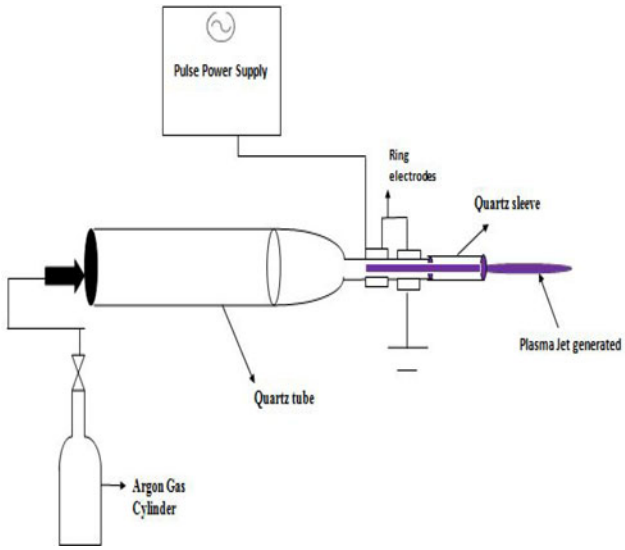

Fig. 2. Schematic diagram of double ring electrode configuration with quartz sleeve.

Figure 4 shows the relationship between the power consumed and supply frequency at different voltages. It is clearly seen that at a lower voltage of 3.5 kV when the frequency is increased from 10 to 25 kHz the power consumption rises as the transit time for electrons decreases from 100 μs ($f =$ 10 kHz) to 40 μs ($f = 25$ kHz) , hence greater accumulation of ions resulting in more power consumed at higher supply frequency. Figure 4 shows the consumed power for a frequency range 10–25 kHz at the supply voltage 3.5 kV. It is observed that at combinations of lower supply voltages and frequency of 3.5 kV and 10 kHz the power consumed is around 0.28 W, whereas at the same voltage level as the supply frequency is increased to 25 kHz the power consumed attains a value of 0.94 W. Hence it can be inferred that as the supply frequency is increased at same lower applied voltage, the power consumed in the plasma jet also increases. It can be observed (see Fig. 4) that at supply voltage 4.5 kV and applied frequency 10 kHz the power consumed is 0.46 W, which is slightly higher than the power consumed at supply voltage 3.5 kV and applied frequency 10 kHz. But, at a higher frequency of 25 kHz the power consumed at 4.5 kV is 0.88 W, which is lower than the power consumed at 3.5 kV/25 kHz (0.94 W), as higher energy electrons are

Fig. 3. Plasma jet generated using double ring electrode configuration.

https://doi.org/10.1017/S0263034616000501 Published online by Cambridge University Press

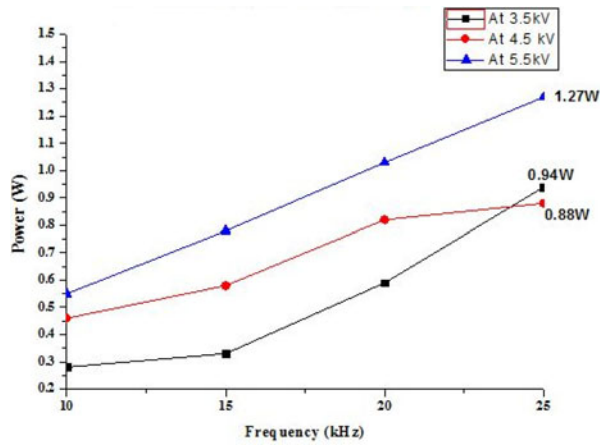

Fig. 4. Power consumption in the jet for different frequencies and 3.5–5.5 kV applied voltage.

already available to cause ionization of argon gas atoms, power consumption is less. It is quite clear that power consumption is not a linear function of frequency at different applied voltages of upto 4.5 kV but however at a higher voltage of 5.5 kV it is found to have a linear relationship. To illustrate it further, a similar graph has also been plotted at higher voltage 5.5 kV and at different frequencies (see Fig. 4). At applied voltage 5.5 kV and frequency 10 kHz the power consumed is 0.55 W. Moreover, there is a significant increment in the power consumed as supply frequency is increased and the peak power consumed by the device reaches 1.27 W at 5.5 kV/25 kHz. This can be attributed to discharge in glow discharge region illustrated in Figure 5, which shows there is only a single peak indicating glow discharge, where uniform discharge happens across entire cathode surface. The obtained peak discharge current at 5.5 kV/25 kHz is 144 mA as shown in Figure 5. This indicates all the power supplied is utilized for the discharge process. However, it is also found from our experimental results that beyond supply voltage of 5.5 kV (irrespective of frequency) results in power being lost in heating of the dielectric tube and heating of argon atoms, which is not desirable process in cold plasma jets and should be avoided.

In another set of experiments the supply frequency was kept constant and argon gas flow rate was fixed as 1 liter/min. Then for each set of supply frequencies starting from 10 to 25 kHz, the supply voltage has been varied from 3.5 to 6 kV and power consumed by the device has been recorded.

Figure 6 shows the relationship between power consumed and the supply voltage at different supply frequencies. It is observed that there is no linear relationship between power consumed and applied voltage at different supply frequencies. At lower supply frequency of 10 kHz initially, there is a marginal increment in power consumed from 0.28 to 0.46 W as the supply voltage is increased from 3.5 to 4.5 kV, which is due to the fact that initially available seed electrons are gaining energy from supplied voltage to cause further ionization of argon atoms. But as the supply voltage is increased to 5.5 kV at same applied frequency 10 kHz, the power consumed reaches a 0.56 W where peak discharge current is 176 mA (see Fig. 7). But as the voltage is further increased to 6 kV there is a decrease in the power consumption by the jet. It implies that there is an optimum limit (supply voltage and frequency) for discharge power in the generated cold plasma jet.

Furthermore (see Fig. 6) at supply frequency of 15 kHz there is a sudden increase in the power consumed as the voltage is increased from 3.5 to 4.5 kV, which is attributed to energy absorbed by the seed electrons, which causes subsequent ionization of argon atoms. But as the voltage is increased to 5.5 kV at same applied frequency of 15 kHz the power consumed reaches 0.78 W. This again implies that there is an optimum limit for discharge power generated in the plasma. The peak discharge current remains same as

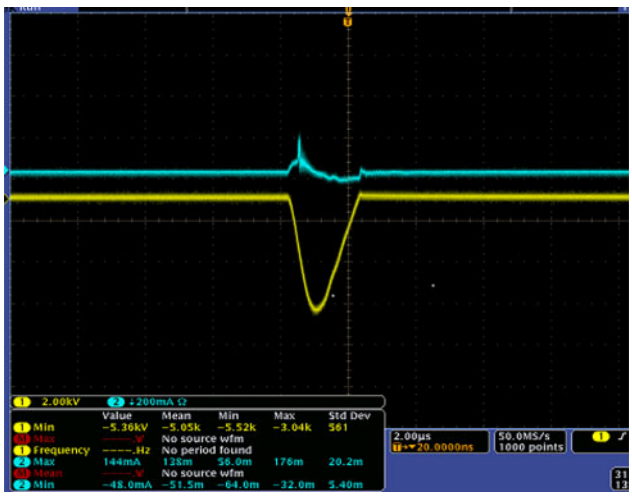

Fig. 5. Oscilloscope current-voltage trace of the cold plasma jet at 5.5 kV/25 kHz.

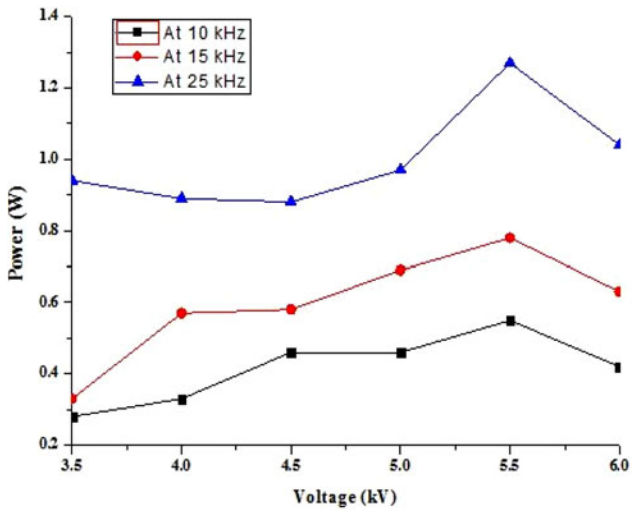

Fig. 6. Power consumption in the jet for different voltages and at 10, 15, and 25 kHz applied frequency.

https://doi.org/10.1017/S0263034616000501 Published online by Cambridge University Press

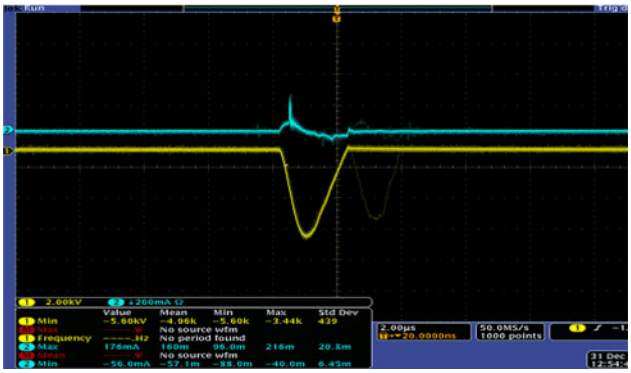

Fig. 7. Peak discharge current of 176 mA at 5.5 kV/10 kHz.

176 mA for both 5.5 kV/15 and 5.5 kV/10 kHz (see Figs 7 and 8).

However (from Fig. 6) at a higher frequency range of 25 kHz initially there is a decrease in the power consumption initially from 0.94 to 0.88 W for increase in supply voltage from 3.5 to 4.5 kV as the seed electrons have already acquired the energy needed to cause further electron avalanche causing ionization of argon gas atoms. But, when the applied voltage reaches 6 kV then the power consumed is 1.04 W since the discharge may approach arc discharge region where the input power is not utilized for glow discharge but it is lost in thermal dissipation of dielectric material (quartz tube) and heating of argon gas (indicated by multiple peaks shown in Fig. 9). This leads to the heating of the dielectric tube. Further, it is observed that above the optimum voltage of 5.5 kV (Fig. 6) at all supply frequencies (10–25 kHz) there is a decrease in power consumed as it is lost in thermal dissipation of dielectric material and heating of argon gas.

The most pivotal factor of a plasma jet length is related to the input supply frequency, voltage, and quartz sleeve. Jet length obtained at different supply voltages has been compared. As mentioned earlier a sleeve is added on top of the nozzle of quartz tube to enhance the jet length by avoiding plasma jet interacting with surrounding air, which consists of electronegative gases and water vapor that impede the propagation of plasma jet. The results of jet length and

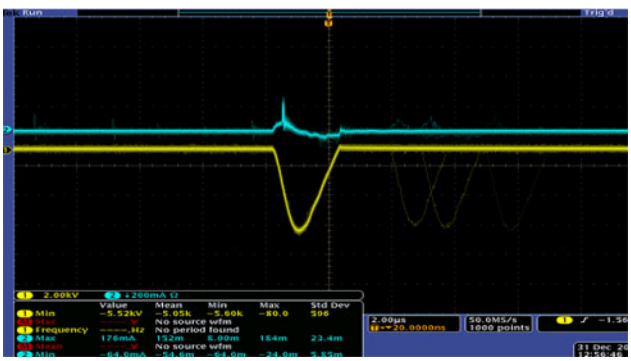

Fig. 8. Peak discharge current of 176 mA at 5.5 kV, 15 kHz.

Fig. 9. Oscilloscope current-voltage trace of the cold plasma jet at 6 kV/25 kHz.

supply frequency (with and without sleeve) at 4.5 kV is shown in Figure 10.

At a lower supply voltage of 4.5 kV and frequency 10 kHz the jet length is 7 mm without the sleeve and it increases to 9 mm with the quartz sleeve. There has been a significant increment in the jet length up to 17 mm obtained with the quartz sleeve compared with a jet length of 12 mm without the sleeve at a supply frequency of 25 kHz. The difference in the jet length is due to the interaction of the plasma with the ambient air. At a low applied voltage, the propagation length of the jet is short as the positive charges will be neutralized by the polarization charges induced in the region of the ground electrode thus limiting its propagation (Jiang *et al.*, 2009).

The results of jet length and supply frequency (with and without sleeve) at 6 kV is shown in Figure 11. At a higher voltage of 6 kV, as shown in Figure 11, even at lower frequency there is a significant difference between the length of plasma jet generated with sleeve and without sleeve, which is 22 and 17 mm, respectively. With this sufficiently large voltage (6 kV), the polarization charges at the ground electrode will get saturated, and they are unlikely to be able to compensate the discharge process. Therefore the charge accumulation region will extend beyond the ground electrode, resulting in an overfall of charges (Jiang *et al.*, 2009). So as the applied voltage increases, more argon

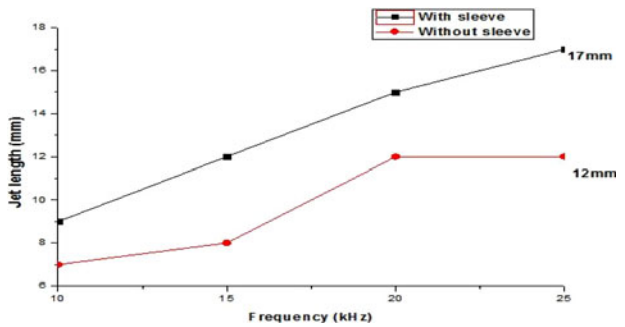

Fig. 10. Jet length versus supply frequency at 4.5 kV.

https://doi.org/10.1017/S0263034616000501 Published online by Cambridge University Press

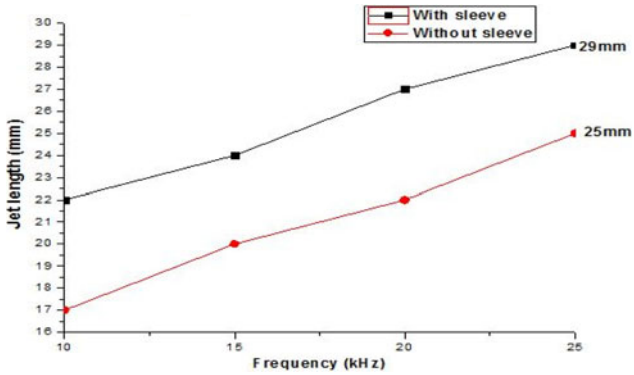

Fig. 11. Jet length versus supply frequency at 6 kV.

energetic species are created and their pronounced energy allows them to penetrate deeper into the surrounding air, leading to the formation of an extended plasma jet. Hence longer jet length is observed at higher applied voltage. The maximum length of the plasma jet obtained is 29 mm at 6 kV/25 kHz with quartz sleeve. The maximum plasma jet length reached without the sleeve is 25 mm due to the interaction of argon ions with surrounding gases of atmosphere consisting of electronegative gases. Nevertheless, there has been a notable increase in jet length (4–16 mm) when the supply voltage is increased from 4.5 to 5.5 kV. The maximum power consumption is at 5.5 kV/25 kHz. The table summarizes the relationship between supply voltage and frequency with respect to peak discharge current, jet length (with and without sleeve), and power consumption by the device is given in Table 1.

Table 1. *Electrical characterization of ring electrode plasma jet*

Supply voltage (kV)	Supply frequency (kHz)	Peak discharge current (mA)	Jet length (mm) without sleeve	Jet length (mm) with sleeve	Power (W)
3.5	10	152	2	5	0.28
4	10	160	4	7	0.33
4.5	10	176	7	9	0.46
5	10	144	12	15	0.46
5.5	10	176	15	21	0.56
6	10	192	17	22	0.42
3.5	15	96	4	7	0.33
4	15	112	6	9	0.58
4.5	15	152	8	12	0.58
5	15	144	14	17	0.69
5.5	15	176	18	23	0.78
6	15	232	20	24	0.63
3.5	20	88	6	10	0.59
4	20	128	8	12	0.73
4.5	20	112	12	15	0.82
5	20	152	18	22	1.12
5.5	20	168	20	25	1.04
6	20	184	22	27	0.72
3.5	25	88	8	12	0.94
4	25	96	11	14	0.89
4.5	25	152	12	17	0.88
5	25	128	22	25	0.97
5.5	25	144	24	28	1.27
6	25	216	25	29	1.04

4. SUMMARY

From our results (see Fig. 4) it is clear that at combinations of lower supply frequency and voltage there is no linear relationship between the power consumed and supply frequency. However at a higher voltage of 6 kV and higher frequency (25 kHz), there seems to be a linear relationship between the power consumed and applied voltage as there is lesser transit time for the electrons (40 μs), which causes ion accumulation resulting more consumption of power with an increase in supply voltage. There is further no linear relationship between the power consumed and applied voltage at different applied supply frequency (10–25 kHz) (see Fig. 6), however it is observed that at all supply frequencies (10–25 kHz) there is peak consumption of power occurring between 5–5.5 kV, but as voltage is increased further to 6 kV there is decrease in the power consumed in all frequencies (10–25 kHz), which signifies that after an optimum voltage of 5–5.5 kV any further increase of voltage results in power dissipated in heating of the dielectric material, which is clearly seen from the occurrence of multiple peaks (Fig. 9). The presence of these multiple peaks indicates that the discharge is approaching arc discharge region. From Table 1 it is clearly observed that peak power consumed at supply frequency (10–25 kHz) occurs between 5 and 5.5 kV with a discharge current (144–176 mA).The peak power consumed by the device is 1.27 W at 5.5 kV/25 kHz with minimal peak discharge current of 144 mA. It is also found from experimental results that for an average power consumption of 0.5–0.9 W the tube should be operated between optimum range 3.5–4.5 kV and 15–20 kHz. It is further observed the power is lost in heating of dielectric material and heating of argon gas atoms beyond a supply voltage of 5.5 kV irrespective of supply frequency. The jet length increases as the supply voltage and frequency increases. However, there is a notable increase in jet length (4–16 mm) when the supply voltage is increased from 4.5 to 5.5 kV. From the results of the electrical characterization of ring electrode configuration, the optimum range established helps in generation of plasma jet without arcing and without any physical damage to the tube, which could occur due to excessive thermal heat dissipation. The developed cold APPJ of greater lengths may be useful for different biological applications.

ACKNOWLEDGMENTS

The authors thank Dean C.E.T (Mody University of Science & Technology) for his valuable support during this research work. The authors are also thankful to Director of Central Electronics Engineering Research Institute for providing the necessary lab facilities in performing these experiments. The authors are greatful to

https://doi.org/10.1017/S0263034616000501 Published online by Cambridge University Press

team members Aditya Sinha and Dharmender for their help during this experimental work at CSIR-CEERI, Pilani.

REFERENCES

Bibinov, N., Dudek, Engemann, J. & Awakowicz, P. (2007). Characterization of an atmospheric pressure dc plasma jet. *J. Phys. D* **40**, 736–742.

Eliasson, B. & Kogelschatz, U. (1991). Nonequilibrium volume plasma chemical processing. *IEEE Trans. Plasma Sci.* **19**, 1063–1077.

Girard-Lauriault, P.-L., Mwale, F., Iordanova, M., Demers, C., Desjardins, P. & Wertheimer, M.R. (2005). Atmospheric pressure deposition of micropatterned nitrogen-rich plasma-polymer films for tissue engineering. In *Plasma Processes and Polymers*, (WILEY-VCH Verlag, Ed.), Vol. 2, pp. 263–270. Weinheim: Wiley.

Jeong, J.Y., Babayan, S.E., Tu, V.J., Park, J., Hicks, R.F. & Selwyn, G.S. (1998). Etching materials with an atmospheric-pressure plasma jet. *Plasma Source Sci. Technol.* **7**, 282–285.

Jiang, N., Ji, A. & Cao, Z. (2009). Atmospheric pressure plasma jet: Effect of electrode configuration, discharge behaviour, and its formation mechanism. *J. Appl. Phys.* **106**, 013308.

Joaquin, J.C., Abramzon, N., Bray, J. & Brelles-Mariño, G. (2006). Biofilm destruction by RF high-pressure cold plasma jet. *IEEE Trans. Plasma Sci.* **34**, 1304–1329.

Kasperczuk, A., Pisarczyk, T., Badziak, J., Borodziuk, S., Chodukowski, T., Parys, P., Ullschmied, J., Krousky, E., Masek, K., Pfeifer, M., Rohlena, K., Skala, J. & Pisarczyk, P. (2010). Interaction of two plasma jets produced successively from Cu target. *Laser Part. Beams* **28**, 497–504.

Laroussi, M. (2002). Nonthermal decontamination of biological media by atmospheric-pressure plasmas: Review, analysis, and prospects. *IEEE Trans. Plasma Sci.* **30**, 1409–1415.

Laroussi, M. & Lu, X.P. (2005). Room-temperature atmospheric pressure plasma plume for biomedical applications. *Appl. Phys. Lett.* **87**, 113902.

Li, L., Liu, C., Zhang, X., Wu, G., Zhang, M., Fu, R.K.Y. & Chu, P.K. (2014). Plasma-target surface interaction during non-equilibrium plasma irradiation at atmospheric pressure: Generation of dusty plasma. *Laser Part. Beams* **32**, 69–78.

Liu & Neiger, M. (2003). Electrical modelling of homogeneous dielectric barrier discharges under an arbitrary excitation voltage. *J. Appl. Phys.* **36**, 1632–1638.

Lu, X.P. & Laroussi, M. (2006). Dynamics of an atmospheric pressure plasma plume generated by sub-microsecond voltage pulses. *J. Appl. Phys.* **100**, 063302.

Pal, U.N., Sharma, A.K., Soni, J.S., Sonu, KR, Khatun, H., Kumar, M., Meena, B.L., Tyagi, M.S., Lee, B-J., Iberler, M., Jacoby, J. & Frank, K. (2009). Electrical modelling approach for discharge analysis of a coaxial DBD tube filled with argon. *J. Appl. Phys.* **42**, 045213.

Park, J. Schutze, A., Jeong, J.Y., Babayan, S.E., Selwyn, G.S. & Hicks, R.F. (1998). The atmospheric-pressure plasma jet: A review and comparison to other plasma sources. *IEEE Trans. Plasma Sci.* **26**, 1685–1694.

Sanchez-Gonzalez, R., Kim, Y., Rosocha, L.A. & Abbate, S. (2007). Methane and ethane decomposition in an atmospheric-pressure plasma jet. *IEEE Trans. Plasma Sci.* **35**, 669–1676.

Stevens, G.C. & Shenton, M.J. (2001). Surface modification of polymer surfaces: Atmospheric plasma versus vacuum plasma treatments. *J. Phys. D* **34**, 2761–2768.

Teschke, M., Kedzierski, J., Finantu-Dinu, E.G., Korzec, D. & Engemann, J. (2005). High-speed photographs of a dielectric barrier atmospheric pressure plasma jet. *IEEE Transactions on Plasma Science* **33**, 310–311.

Xiong, Q., Lu, X., Ostrikov, K., Xiong, Z., Xian, Y., Zhou, F., Zou, C., Hu, J., Gong, W. & Jiang, Z. (2009). Length control of He atmospheric plasma jet plumes: Effects of discharge parameters and ambient air. *Phys. Plasmas* **16**, 043505.

Xu, G.-M., Ma, Y. & G.-J. Zhang (2008). DBD plasma jet in atmospheric pressure argon. *IEEE Trans. Plasma Sci.* **36**, 1352–1353.